Centralized Dynamics Multi-frequency GNSS Carrier Synchronization

Padma Bolla, Jordi Vilà-Valls, Pau Closas and Elena Simona Lohan

Abstract—In this article we propose a new centralized multi-frequency carrier tracking architecture using an adaptive Kalman filter to enhance the loop sensitivity and reliability of the individual signal tracking in challenging signal environment. The central task of the centralized dynamics-tracking filter is to effectively blend multiple frequency carrier phase observations in order to estimate the common geometric Doppler frequency of multiple-frequency received signals. Conventionally, multi-frequency signals are tracked independently with a fixed-loop noise bandwidth tracking approach, which is sub-optimal in time-varying signal environments. A suitable collaboration in multiple-frequency signal tracking using a centralized dynamics-tracking loop enables a robust carrier tracking even if some of the frequency channels are affected by ionospheric scintillation, carrier-phase multipath, or interference. Additionally, computational efficiency of the multiple-frequency tracking improves by using the proposed tracking loop architecture. Performance of the proposed multi-frequency tracking-loop architecture is verified with experiments using live multi-frequency satellite signals collected from GPS Block-IIF satellites under the influence of frequency-selective interference signals.

Index Terms—Multi-frequency GNSS tracking, Adaptive Kalman filter, Interference

I. INTRODUCTION

Currently, the envisaged multi-frequency GNSS signals are designed to offer several services and to meet the performance and integrity requirements of a wide categories of civilian users. Each frequency signal is designed with unique signal characteristics, suitable for an intended civilian application and allocated to separate Radio Frequency (RF) spectrum in the L-band. The multiple-frequency signal transmission has opened a new avenue to potential ways of using geometry-free combinations of two or more code- and carrier-phase observations, to eliminate ionosphere delay [1] and to use in the carrier-phase integer ambiguity resolution [2].

In a conventional multi-frequency receiver, multiple signals are tracked independently by means of standard code- and carrier-tracking loops, using delay-locked loops (DLL) and frequency/phase-locked loops (FLL/PLL), respectively. The pseudorange observables, which rely on the delay measurements of the code-tracking loop, are limited in terms of precision by the wavelength of the code and carrier signal. Because

of the independence of the tracking loops, the precision in multi-frequency linear combination of observations is limited by the lower precision of the multiple signals. In order to get mutual benefits of multiple-frequency signals and to improve the computational efficiency in signal processing, a suitable collaboration across multiple frequency signal processing can be explored, which is the motivation of the current research work.

The multiple-frequency signals transmitted from the same satellite are subject to both deterministic and non-deterministic disturbances while propagating through the atmosphere, which cause code- and carrier-phase variations in the received signal. Some of these changes are common across multiple frequency signals, while some are specific to each frequency channel. The line-of-sight (LOS) relative movement between the satellite and receiver causes signal code- and carrier-phase variations which are common across the multiple frequency signals. Besides the common geometric phase variations, there are also channel-specific phase variations which are not common to the other channels and change the code and carrier phase in an independent manner. The inherent linear relationship between multiple frequency signals which are synchronously generated from the same reference clock can be used to track the common-platform signal dynamics using a centralized tracking-loop scheme. Then, the effort to track the LOS platform dynamics with individual frequency channel PLLs can be reduced. This will enable the bandwidth of the PLL to be reduced and, thus, it will improve the noise performance in each frequency channel.

The collaboration in multiple satellite signal tracking using coupled-tracking channels was initially introduced in [3] for improved signal tracking performance in weak signal environment. The robustness of tightly coupled multi-satellite signal tracking for precise positioning applications was demonstrated in [4]. The space-diversity techniques such as coupled vector tracking loop (VTL) are well-known procedures in GNSS receivers [5]. The space-diversity techniques enhance the individual satellite signal tracking sensitivity in weak signal environment by making use of redundancy of satellite signals. The VTL was introduced in [6] for the DLL, and then the same concept was extended to joint carrier tracking of multi-constellation satellite signals using vector phase-locked loop (VPLL) in [7]. Different variants of the VTL architecture have been proposed by many research groups [8], [9], and the integrity of VTL techniques has been an active research topic in the past decade. A VPLL for joint tracking of multiple frequencies and multiple satellites was presented in [10] to improve the carrier-tracking loop robustness by mapping the tracking errors into position error, clock drift, ionospheric, and

P. Bolla is with Samara National Research University, Samara, Russia; J. Vilà-Valls is with ISAE-SUPAERO, University of Toulouse, 31055 Toulouse, France; P. Closas is with the Electrical and Computer Engineering Department, Northeastern University, Boston, MA, USA; E.S. Lohan is with the Tampere University of Technology (to become Tampere University from Jan 2019), Tampere, Finland; E-mail: padmabolla@ssau.ru, jordi.vila-valls@isae-supaero.fr, closas@northeastern.edu, elena-simona.lohan@tut.fi

tropospheric errors. The well-known limitation of VTLs is the propagation of position errors in the navigation filter to all the tracking channels [11] and inadequate update rate of the navigation filter. From the past decade, with the availability of multiple-frequency signals from the same satellite, frequency-diversity techniques, such as inter band Doppler aiding, have been used to improve the individual signal tracking sensitivity in challenging signal environments. Recent research in [12] has shown tracking performance improvements in fading signal scenarios using combined correlator outputs based on two frequency channel tracking. Work in [13] proposed a combined multi-frequency signal tracking using a Kalman filter (KF) to improve the tracking loop performance under ionospheric scintillation. Notice that most of the work related to multi-frequency signal tracking in the past addressed selective signal environments.

In this paper we propose a computationally efficient and robust multi-frequency tracking architecture suitable for all signal conditions. In real GNSS signal environments, multiple frequency signals from the same satellite often experience interference either at the same time instant (concurrently) or at different time instants (non-concurrently). The concurrent interference is due to shadowed satellites in urban canyon and indoors, while non-concurrent frequency selective interference is due to multipath or intentional meaconing/jamming/spoofing. To improve tracking loop performance in such challenging signal environments, we propose a centralized multi-frequency signal dynamics tracking loop (CTL) architecture using an adaptive KF (AKF). The central task of the CTL is to blend multiple frequency carrier phase measurements to track common geometric Doppler shifts in the received multiple frequency signals. Additionally, a narrow bandwidth PLL is employed in each frequency channel to track the residual carrier phase variations specific to each channel. The CTL AKF provides the geometric Doppler frequency estimate to individual PLLs to tune their respective carrier oscillator. Two approaches are proposed to use multiple frequency signal carrier phase measurements in order to improve tracking loop sensitivity in concurrent and non-concurrent frequency selective interference scenario. In concurrent interference signal conditions, optimally weighted linear combinations of multiple signal phase observations are used to estimate LOS signal dynamics, while in non-concurrent interference scenarios, stronger signal phase measurements are used. The carrier-to-noise power ratio (C/N_0) estimator in each frequency channel is used to sense the signal environment and for measurement model switching in the AKF.

A suitable collaboration in multiple frequency signal tracking offers many benefits in terms of accuracy, integrity and robustness, even if some of the frequencies are affected by ionosphere scintillations, multipath, or interferences. The multiple frequency signal tracking using the CTL allows the bandwidth reduction in individual signal carrier tracking loops by eliminating the need to track the platform dynamics. Hence, this integrated tracking loop results in precise carrier phase observations and improved dynamic performance. Additionally, the CTL provides a means to detect frequency selective interference and an isolation scheme that can be used to verify the quality of carrier phase observations.

The paper is organized as follows: in Section II, GNSS multi-frequency signal tracking is discussed in detail using conventional tracking loop architecture; in Section III, the proposed CTL architecture is introduced, and the AKF tuning methodology is detailed; in Section IV, the performance of the new CTL is analyzed; experimental results are shown in Section V; finally, conclusions about the proposed CTL architecture are given in section VI.

II. GNSS MULTI-FREQUENCY SIGNAL CARRIER TRACKING

The multi-frequency GNSS signals incident on the receiver's antenna can be represented as a composite sum of individual frequency signals plus noise at the specified frequency band k,

$$s(t) = \sum_{k=1}^{N} \left(\sqrt{2P_k} C_k(t-\tau_k) D_k(t-\tau_k) e^{j2\pi(f_{L_k}(t)t+\phi_k(t))} \right) + n_k(t),$$
(1)

where P_k is the received signal power; $C_k(t)$ is the pseudo-random code; $D_k(t)$ is the navigation message data bits; τ_k is the transition delay from satellite to the receiver; $f_{L_k}(t)$ is the signal carrier frequency and $\phi_k(t)$ is the signal carrier-phase; Finally, $n_k(t)$ is the noise specific to an individual signal frequency band. The received signal carrier phase $\phi_k(t)$ represents the signal phase dynamics, including satellite induced Doppler, Doppler drift and user-dynamic induced phase variations. The received signal carrier phase can be represented using Taylor's approximation as,

$$\phi_k(t) = \phi_k(t_0) + T\dot{\phi}_k(t_0) + \frac{T^2}{2}\ddot{\phi}_k(t_0) + \varepsilon_{\phi_k},$$
(2)

where $\phi_k(t_0)$, $\dot{\phi}_k(t_0)$ and $\ddot{\phi}_k(t_0)$ are the received signal phase and its time derivatives at t_0 in cycles, cycles/s and cycles/s^2 respectively; $T = t - t_0$, is the signal integration time; ε_{ϕ_k} is the error in the approximation. The rate of change of phase is simply the Doppler frequency of the signal, hence, (2) can be written as,

$$\phi_k(t) = \phi_k(t_0) + Tf_{D_k}(t_0) + \frac{T^2}{2}\dot{f}_{D_k}(t_0) + \varepsilon_{\phi_k},$$
(3)

where $f_{D_k}(t_0)$ and $\dot{f}_{D_k}(t_0)$ are the Doppler frequency and the rate of Doppler frequency in cycles/s and cycles/s^2, respectively;

Typically, the code and carrier frequencies of multiple frequency signals from the same satellite are synchronously generated from a common reference clock. For instance, GPS L1, L2C, and L5 signals are generated synchronously from the reference clock frequency, $f_{ref} = 10.23$ MHz. Hence, the three signal code and carrier frequencies are linearly related to f_{ref} as,

$$\begin{aligned} f_{L_k} &= \alpha_k f_{ref} \; ; \; f_{cL_k} = \beta_k f_{ref} \; ; \; k = \{1, 2, 5\} \\ \alpha_1 &= 154, \quad \alpha_2 = 120, \quad \alpha_5 = 115, \\ \beta_1 &= \beta_2 = 1/10, \quad \beta_5 = 1, \end{aligned}$$
(4)

where f_{L_k} and f_{cL_k} are the carrier and code frequencies of subscripted GPS L-band signals.

The received multi-frequency GNSS signal code and carrier-phase variations are subjected to deterministic and non-deterministic disturbances due to many error sources in the propagation channel. Some of these disturbances are common across multiple frequency signals, while some are specific to each frequency channel. The common phase variations are due to LOS relative movement between the satellite and receiver. The channel specific phase variations are due to frequency dependent error sources such as ionosphere Total Electron Content (TEC) variations and receiver reference clock frequency drift.

Then, the received satellite signal frequency deviation f_{D_k} includes the Doppler frequency due to LOS geometric shift, changes in the total electron (TEC) content of the ionosphere layer and drift in the reference clock frequency of the receiver with respect to the satellite clock. The geometric Doppler shift depends on the relative movement between the satellite and receiver, while the ionospheric Doppler shift depends on the signal propagation path through the atmosphere [14]. The Doppler frequency due to reference clock frequency drift is introduced through down conversion and sampling process at the RF front-end [15]. The received satellite signal carrier frequency deviation at the k-th frequency channel can be represented as a combination of geometric Doppler shift f_{GD_k} and the residual Doppler shift f_{RD_k} due to ionospheric Doppler shift f_{ID_k} and reference clock Doppler shift f_{CD_k},

$$f_{D_k} = f_{GD_k} + f_{RD_k}, \tag{5}$$
$$f_{RD_k} = f_{ID_k} + f_{CD_k}.$$

The geometric Doppler shift is significantly higher than the residual Doppler shift due to ionosphere TEC changes and drift in the reference clock frequency.

A. LOS - dynamics

The geometric Doppler frequency can be expressed as the velocity of the receiver relative to the transmitter in the LOS direction, scaled by the carrier wavelength. This relation can be expressed as,

$$f_{GD_k} = \frac{1}{\lambda_{L_k}} (\mathbf{v}_R - \mathbf{v}_S) \mathbf{u}_{LOS}, \tag{6}$$

$$\lambda_{L_k} f_{GD_k} = (\mathbf{v}_R - \mathbf{v}_S) \mathbf{u}_{LOS} = \delta\dot{\rho}$$

where λ_{L_k} is the wavelength of the carrier signal at subscripted frequency channel; $\mathbf{v}_R$ and $\mathbf{v}_S$ are receiver and satellite velocities in the LOS direction, respectively; $\mathbf{u}_{LOS}$ is the unit LOS vector from the receiver to the satellite; $\delta\dot{\rho}$ is the range rate of the signal. The LOS Doppler shift is in the range of ± 5 kHz for static receiver and ± 10 kHz for dynamic receiver

From (4) and (6), the geometric Doppler shift in the code and carrier frequencies of three GPS civil signals is linearly related as,

$$\lambda_{L_1} f_{GD_{L_1}} = \lambda_{L_2} f_{GD_{L_2}} = \lambda_{L_5} f_{GD_{L_5}} \tag{7}$$

$$\lambda_{c_{L_1}} f_{cd_{L_1}} = \lambda_{c_{L_2}} f_{cd_{L_2}} = \lambda_{c_{L_5}} f_{cd_{L_5}}$$

where $\lambda_{c_{L_k}}$ is the wavelength of the code frequency; f_{cd_k} and f_{GD_k} are the geometric Doppler shift in the code and carrier frequency of the subscripted frequency channel.

From (6) it is inferred that the LOS Doppler shift in each frequency channel is common and can be obtained from the Doppler shift or range rate of the other co-existing frequency signals with appropriate scaling with the wavelength of the received signal carrier frequency.

B. Ionosphere TEC - dynamics

The changing TEC in the ionosphere layer results in an additional ionospheric Doppler shift f_{ID_k} in the received satellite signal, which is relatively small compared to the geometric Doppler shift, and can be computed as [14],

$$f_{ID_k} = \frac{1.34 \times 10^{-7}}{f_{L_k}} \left(\frac{\partial(TEC)}{\partial t} \right). \tag{8}$$

As shown in [14], an upper limit to the rate of change of TEC to the stationary user is approximately $0.1 \times 10^{16} \left(\frac{el}{m^2}/s \right)$, which results in an additional frequency shift of $0.085/0.1/0.1$ Hz at L1/L2/L5 frequencies. From (8), we can see that the ionospheric Doppler shift is a frequency dependent error.

C. Reference oscillator - dynamics

The frequency fluctuations of the main reference oscillator, which is used to generate reference signal in the receiver, causes a Doppler shift in the down converted received signal. The reference oscillator is sensitive to the receiver platform dynamics, such as acceleration and jerk. This causes the oscillator frequency to drift over a time, which will directly result in a Doppler shift in the reference signal frequency at the receiver. The drift in the reference oscillator frequency subject to the acceleration dynamics is [15],

$$\Delta f_{ref} = s_g f_{ref} a_g \tag{9}$$

where a_g is the acceleration in units of g, $g = 9.8$ m/s^2; f_{ref} is the reference clock frequency; s_g the reference oscillator sensitivity to the acceleration, which varies with the type of reference oscillator. Typical values of acceleration sensitivity are, $s_g = 5 \times 10^{-9}/g$ for a TCXO, or $s_g = 3.5 \times 10^{-9}/g$ for an OCXO. The drift in the reference clock frequency corresponds to a Doppler shift in the reference carrier signal f_{L_k}, which can be expressed as,

$$f_{CD_k} = s_g f_{L_k} a_g. \tag{10}$$

For instance, at an acceleration of $a_g = 1g$, the Doppler shift in L1/L2/L5 reference clock frequency generation is about $7.8/6.2/5.8$ Hz using a TCXO and $5.5/4.2/4.1$ Hz using an OCXO. From (10) it is inferred that the influence of reference oscillator Doppler shift also depends on the received signal frequency.

The received multiple frequency signals are down converted to baseband using RF front end. The down-converted signal is subsequently sampled and quantized to produce digital complex in-phase (I) and quadrature-phase (Q) signal. The digitized complex baseband data will be further processed in a digital signal processing module in three stages: acquisition, tracking, and navigation blocks. The acquisition is a onetime process, that coarsely estimates the code-phase and carrier Doppler frequency of visible satellites signal. Subsequently,

the code and carrier phase variations of multi-frequency signals are tracked using independent tracking loops in standard tracking loop architecture, which is discussed in the following section.

D. Standard multi-frequency tracking loop architecture

A conventional multi-frequency GNSS receiver has multiple individual signal code and carrier tracking channels, each one tracking a single frequency signal received from the satellite [11]. Fig. 1 illustrates the standard code and carrier tracking loop architecture for multiple frequency channels. The code/carrier phase tracking loop in each frequency channel is build up with a complex correlator (mixer and integrator), code/carrier phase discriminator (PD), code/carrier loop filter and code/carrier numerically controlled oscillator (NCO). Each tracking channel synchronizes the receiver reference signal code and carrier frequency with that of the received satellite signal, by controlling the reference signal code and carrier frequency generator.
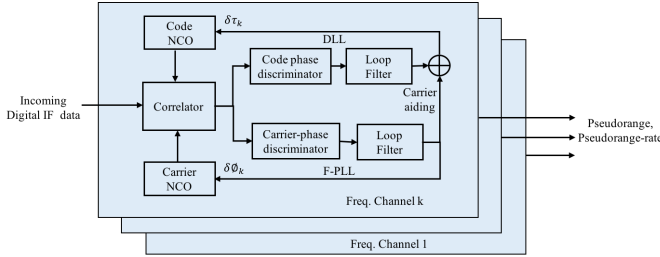

Figure 1: Standard signal tracking loop for single frequency channel

After the received signal is correlated with the local reference signal, the resultant baseband signal prompt correlator output has two components in each frequency channel k: In-Phase IP_k and Quadrature phase QP_k,

$$IP_k = R(\delta\tau_k)\cos(\pi\delta f_{D_k} + \delta\phi_k), \tag{11}$$
$$QP_k = R(\delta\tau_k)\sin(\pi\delta f_{D_k} + \delta\phi_k),$$

where $R(\delta\tau_k)$ is the cross-correlation function between the received and reference signal; $\delta\tau_k$, $\delta\phi_k$ and δf_{D_k} are the mean code phase, carrier phase and carrier frequency errors between the received and replica signals, respectively.

In the PLL carrier tracking loop, the average phase difference between the received and reference signals is,

$$\delta\phi_k(t) = \phi_k(t) - \hat{\phi}_k(t) \tag{12}$$
$$\delta\phi_k(t) = \delta\phi_k(t_0) + T\delta f_{D_k}(t_0) + \frac{T^2}{2}\delta\dot{f}_{D_k}(t_0) + \delta\varepsilon_{\phi_k},$$

where $\delta f_{D_k} = \delta f_{GD_k} + \delta f_{RD_k}$ is total Doppler frequency error in each frequency channel, δf_{GD_k} is the geometric Doppler frequency error, $\delta f_{RD_k} = \delta f_{ID_k} + \delta f_{CD_k}$ is the residual Doppler frequency error due to ionosphere TEC variations and reference clock drift. From the complex prompt correlator outputs (IP_k, QP_k), the phase and frequency errors

in a non-coherent PLL using a two-quadrant arctangent phase discriminator can be computed as [16],

$$e_{\phi_k} = \tan^{-1}\left(\frac{QP_k}{IP_k}\right) + n_{\phi_k}, \tag{13}$$
$$e_{f_k} = \delta\phi_k(t) - \delta\phi_k(t-1) + n_{f_k},$$

where n_{ϕ_k} and n_{f_k} are the phase and frequency error measurement noise, respectively.

The phase and frequency error measurement from the non-linear phase discriminator output will be processed by the PLL loop filter to estimate the phase and frequency difference between the received and reference signals.

1) Design parameters of carrier tracking loop filter: the PLL loop filter order is selected based on the expected signal dynamics. The second order FLL assisted third order PLL is preferable to bear jerk type of dynamics. For a single frequency channel, an FLL assisted PLL (F-PLL) carrier tracking loop filter can be written using an error state variable model as [17]

$$\delta\mathbf{x}_{t+1} = \mathbf{F}\delta\mathbf{x}_t + \mathbf{FL}\mathbf{z}_{t+1}, \tag{14}$$

where $\mathbf{z}_{t+1} = [e_{\phi_k}, e_{f_k}]_{t+1}^\top$ and

$$\mathbf{F} = \begin{bmatrix} 1 & T & \frac{T^2}{2} \\ 0 & 1 & T \\ 0 & 0 & 1 \end{bmatrix},$$

and $\delta\mathbf{x}_t = [\delta\phi_k, \delta f_{D_k}, \delta\dot{f}_{D_k}]_t^\top$ are the carrier phase error, Doppler frequency error and Doppler rate error in cycles, cycles/s and cycles/s^2, respectively. The fixed gain matrix $\mathbf{L} = \begin{bmatrix} \alpha_1 & \alpha_2 & \alpha_3 \\ 0 & \beta_1 & \beta_2 \end{bmatrix}^\top$ depends on FLL and PLL loop bandwidth and the coherent integration time; α_i and β_i are the PLL and FLL filter gain coefficients, respectively.

The receiver F-PLL phase and frequency difference measurements have two major error sources: thermal noise error σ_τ, and steady state dynamic tracking errors, ϕ_e and f_e.

The F-PLL tracking loop 1-sigma threshold rule is [16],

$$\sigma_{\delta\phi} = \sigma_{\tau_{pll}} + \frac{\phi_e}{3} \leq 0.26 \text{ [cycles] for the PLL} \tag{15}$$
$$\sigma_{\delta f} = \sigma_{\tau_{fll}} + \frac{f_e}{3} \leq \frac{1}{12T} \text{ [Hz] for the FLL}$$

The 1-sigma values of thermal noise in the PLL and FLL can be expressed as a function of carrier tracking loop bandwidths B_{pll} and B_{fll}, loop update interval T, and carrier-to noise ratio C/N_0 ($= 10^{0.1C/N_0}$ for C/N_0 in dB-Hz),

$$\sigma_{\tau_{pll}} = \left(\frac{1}{2\pi}\right)\sqrt{\frac{B_{pll}\left(1 + \frac{1}{2TC/N_0}\right)}{C/N_0}} \text{ [cycles]} \tag{16}$$
$$\sigma_{\tau_{fll}} = \left(\frac{1}{2\pi T}\right)\sqrt{\frac{4B_{fll}\left(1 + \frac{1}{TC/N_0}\right)}{C/N_0}} \text{ [Hz]}$$

The 1-sigma values of the steady state dynamic tracking bias error for the second order PLL and FLL are

$$\phi_e = \frac{(\delta\ddot{\phi})}{w_L^2} = 0.2809 \frac{\delta\dot{f}}{B_{pll}^2} \quad [\text{cycles}] \qquad (17)$$

$$f_e = \frac{(\delta\dddot{\phi})}{w_L^2} = 0.2809 \frac{\delta\ddot{f}}{B_{fll}^2} \quad [\text{Hz}]$$

where $\delta\dot{f}$ and $\delta\ddot{f}$ are the maximum LOS acceleration and jerk dynamics, [cycles/s^2] and [cycles/s^3], respectively, and w_L is the natural frequency of F-PLL, $w_L = 0.53 B_{pll}/0.53 B_{fll}$ for the second order filters ; B_{pll} and B_{fll} are the loop bandwidth of the PLL and FLL tracking loops, respectively.

The carrier phase and frequency errors are function of the tracking loop bandwidths, B_{pll} and B_{fll}, integration time, T, received signal strength, C/N_0, and signal dynamics, $\delta\dot{f}$ and $\delta\ddot{f}$. The received signal conditions can not be controlled, hence, the equivalent noise bandwidth in the PLL and FLL has to be chosen to accommodate the expected signal dynamics for a given C/N_0 level and signal integration time. The optimal tracking loop bandwidth conditioned on the minimization of tracking loop phase and frequency error can be obtained by differentiating $\sigma_{\delta\phi}$ and $\sigma_{\delta f}$ with respect to loop bandwidth and equating it to zero, i.e., $\frac{\partial\sigma_{\delta\phi}}{\partial B_{pll}} = 0$ and $\frac{\partial\sigma_{\delta f}}{\partial B_{fll}} = 0$. This yields the following optimal bandwidth expression for the PLL and FLL,

$$B_{pll} = \left(\frac{(2.35\delta\dot{f})^2}{\frac{1}{C/N_0}\left(1 + \frac{1}{2TC/N_0}\right)} \right)^{1/5}, \qquad (18)$$

$$B_{fll} = \left(\frac{(2.35\delta\ddot{f})^2}{\frac{4}{C/N_0}\left(1 + \frac{1}{2TC/N_0}\right)} \right)^{1/5}.$$

Analytical values of the optimal PLL tracking loop bandwidth for varying signal power levels, signal dynamics and integration time $T = 20$ ms are shown in Fig. 2.
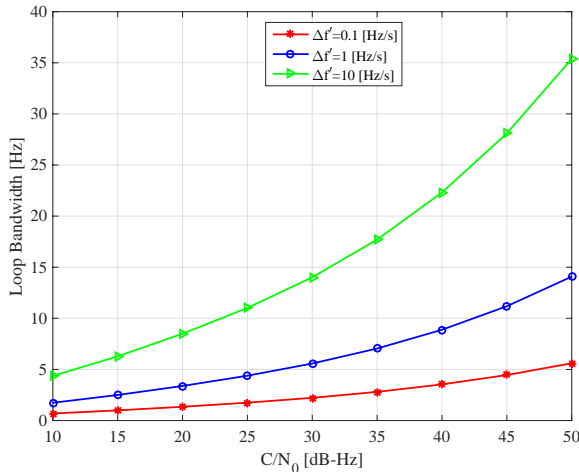

Figure 2: Optimal PLL loop bandwidth for varying C/N_0 and signal dynamics.

A narrow loop bandwidth is beneficial at low C/N_0 levels to improve tracking loop noise performance at low signal dynamics, while the wide loop bandwidth is suitable to track high signal dynamics. Finally, the objective of the tracking loop design criteria is to select the lowest bandwidth that is required to accommodate the expected signal dynamics and to meet the tracking loop error criteria. Hence, for efficient tracking loop operation, the noise bandwidth should be adapted to the received signal C/N_0 value and the changing signal dynamics in real time. For this reason, an adaptive scheme is needed to effectively change the equivalent noise bandwidth with respect to the signal C/N_0 value and signal dynamics estimated using the signal carrier phase error measurements. There are many approaches to realize adaptive tracking loop with respect to changing signal environment as discussed in [18].

It is to be noted that the C/N_0 tracking threshold for three GPS civil signals varies based on the individual signal characteristics and RF channel effects. The GPS L5 signal with high received power and a pilot tracking channel has a high signal tracking sensitivity with low C/N_0 tracking threshold requirement. A suitable collaboration in multiple frequency signal tracking loops improves the individual signal tracking sensitivity, robustness and computational efficiency. However, in conventional multi-frequency tracking loop architectures, the inherent linear relationship between multiple frequency signals that are synchronously generated from the same reference clock in the satellite is neglected. By considering the optimal tracking loop design criteria, and to address some of the limitations in conventional multi-frequency tracking loop architectures, we propose a collaborative multiple-frequency signal tracking using a CTL architecture, as discussed in the following section.

III. CENTRALIZED MULTI-FREQUENCY DYNAMICS TRACKING LOOP ARCHITECTURE

The idea of the CTL is based on the fact that the high frequency component of Doppler shift in the received satellite signal frequency due to LOS platform dynamics is common across multiple frequency signals received from the same satellite. This common signal dynamics information can be estimated by means of a centralized dynamic tracking filter, then, an effort to track them with individual frequency channel PLL can be reduced. This will enable the PLL bandwidth to be reduced, and thus improve the noise performance in each frequency channel. Hence, a CTL filter can be employed to track common carrier phase variations and also to improve the computational efficiency in multiple frequency signal tracking. Additionally, each frequency channel needs a narrow bandwidth PLL to track the residual phase variations due to frequency dependent error sources, such as ionosphere TEC changes and reference clock drift, as discussed earlier. An appropriate loop bandwidth to use in the PLL of each frequency channel can be obtained from a prior estimation of the residual phase error.

The CTL needs to be initialized by the standard carrier tracking loop (STL), which was described in the previous section. Once all the PLLs in the STL are in phase lock, the CTL starts its operation. Fig. 3 illustrates the CTL architecture,
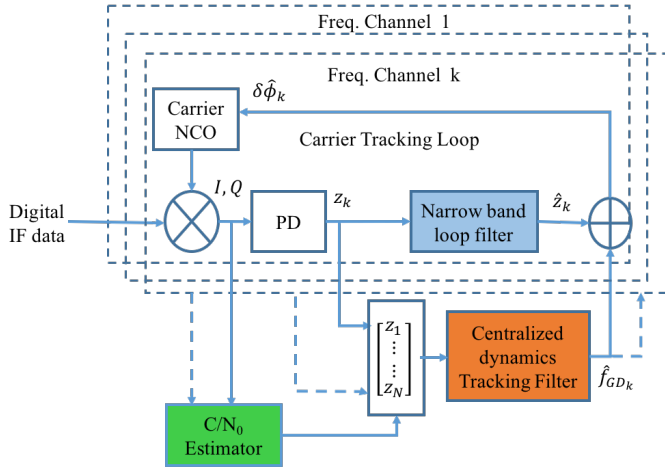
Figure 3: Centralized Multi-frequency carrier tracking loop architecture

which considers a set of closed-loop narrow bandwidth PLLs and a common signal dynamics tracking loop filter. The code phase in multiple frequency channels is tracked by employing independent PLL assisted DLLs.

The CTL computes the common LOS signal dynamics information using a weighted linear combination of carrier phase and frequency error measurements from multiple frequency channels in a coordinated manner. The sum of the LOS geometric Doppler frequency information provided by the CTL and the residual phase and frequency errors tracked by each frequency channel will be used to tune the carrier NCO in each channel,

$$\delta\hat{\phi}_k = \hat{z}_k + \delta\hat{f}_{GD_k} \quad [\text{Hz}] \tag{19}$$
$$\hat{z}_k = \delta\hat{\phi}_0 + \delta\hat{f}_{RD_k} \quad [\text{Hz}]$$

where $\delta\hat{\phi}_k$ is the total control input to carrier oscillator; $\hat{z}_k$ is the estimate of filtered residual phase and frequency error due to frequency dependent error sources in subscripted frequency channel; $\delta\hat{f}_{GD_k}$ is the geometric Doppler shift in frequency provided by the CTL.

By the law of noise variance propagation, the noise in the control input to the carrier NCO can be expressed as,

$$\sigma^2_{\delta\hat{\phi}_k} = \sigma^2_{\hat{z}_k} + \sigma^2_{\delta\hat{f}_{GD_k}} \tag{20}$$

From (20), it is inferred that there is an extra noise induced from the CTL. The extra noise $\sigma^2_{\delta\hat{f}_{GD}}$ induced from the CTL has both systematic and random error components, and is correlated across multiple frequency signal tracking loop phase observations. The correlated observation errors in multiple frequency channels tend to cancel in linear combinations of pseudo-range observations, such as ionosphere free and wide-lane [19]. The centralized dynamics tracking filter can be realized using a conventional higher order fixed bandwidth loop filter. However, for efficient tracking loop operation in time-varying signal environments, the noise bandwidth needs to be adapted to the received signal C/N_0 values and the changing signal dynamics in real time. The AKF is considered

as most suitable solution to adapt to the changing signal environment [20], which is discussed in the following section.

A. Centralized signal dynamics tracking via AKF

The KF is chosen to effectively blend multiple frequency channel carrier phase observations and to track common LOS signal dynamics of the received multiple frequency signals. The signal tracking KF is regarded as identical to the DPLL with time-varying noise bandwidths that optimally enhance the receiver tracking performance in response to user signal environments [21], [17]. Several state-space formulations to design a KF-based signal tracking exist, depending on the measurement variables and the state to be estimated. The measurement vector in the carrier tracking loop can be defined in two ways. In the first approach, the complex correlator output can be directly used as a measurement. In this case, the relationship between measurements and parameters to be estimated is non-linear, which can be solved via an extended KF (EKF). An alternative approach is to use phase discriminator outputs as measurements, which is adopted in the current research work to make use of the conventional tracking loop measurements. The limitation of this approach is that the measurement noise is no longer an additive white Gaussian noise (AWGN). The nonlinear phase discriminator function causes the loss of the AWGN properties if the phase error crosses the linear range of phase discriminator.

In the proposed multi-frequency signal dynamics tracking loop architecture, the KF is replacing the FLL-assisted PLL loop filter in conventional architectures in order to estimate the LOS carrier phase error variations in received multiple frequency signals, based on the multiple-frequency signal phase and frequency error measurements.

The linear state dynamic model for the error-state KF can be written as,

$$\delta\mathbf{x}_{t+1} = \mathbf{F}\delta\mathbf{x}_t + \mathbf{\Gamma}w_t, \tag{21}$$

where $\delta\mathbf{x}_t$ is the $n \times 1$ error-state vector at epoch t; $\mathbf{F}$ is the $n \times n$ non-singular state transition matrix from epoch t to $t+1$; $\mathbf{\Gamma}$ is the $n \times 1$ noise gain vector; w_i is the zero mean additive white Gaussian process noise sequence with variance $\sigma^2_{w_t}$.

The state dynamic model in the centralized multi-frequency signal dynamics tracking KF is assumed to be a discrete Wiener process acceleration model [22] to bear jerk type of dynamics, where the states are the carrier phase error, frequency error and frequency rate error. The error-state dynamic model can be transformed to range domain by scaling with the wavelength as,

$$\begin{bmatrix} \delta\phi_k \\ \delta f_{D_k} \\ \delta\dot{f}_{D_k} \end{bmatrix}_{t+1} \lambda_k = \begin{bmatrix} 1 & T & \frac{T^2}{2} \\ 0 & 1 & T \\ 0 & 0 & 1 \end{bmatrix} \begin{bmatrix} \delta\phi_k \\ \delta f_{D_k} \\ \delta\dot{f}_{D_k} \end{bmatrix}_t \lambda_k + \begin{bmatrix} \frac{T^2}{2} \\ T \\ 1 \end{bmatrix} w_t \lambda_k, \tag{22}$$

The KF error-state vector can be written in the range domain as,

$$\begin{bmatrix} \delta\rho \\ \delta\dot{\rho} \\ \delta\ddot{\rho} \end{bmatrix}_{t+1} = \begin{bmatrix} 1 & T & \frac{T^2}{2} \\ 0 & 1 & T \\ 0 & 0 & 1 \end{bmatrix} \begin{bmatrix} \delta\rho \\ \delta\dot{\rho} \\ \delta\ddot{\rho} \end{bmatrix}_t + \begin{bmatrix} \frac{T^2}{2} \\ T \\ 1 \end{bmatrix} w_t \lambda_k, \tag{23}$$

In this model, the white noise process w_t represents the acceleration increment over the sampling period. The covariance of the process noise multiplied by the gain, $\mathbf{\Gamma} w_t$, is

$$\mathbf{Q}_t = \mathbf{\Gamma} \sigma_{w_t}^2 \mathbf{\Gamma}^\top = \begin{bmatrix} \frac{T^4}{2} & \frac{T^3}{2} & \frac{T^2}{2} \\ \frac{T^3}{2} & T^2 & T \\ \frac{T^2}{2} & T & 1 \end{bmatrix} q_t \, \lambda_k^2 \qquad (24)$$

where $q_t = \sigma_{w_t}^2$ is the process noise acceleration variance in $cycles^2/s^4$. For this model, the practical range of σ_{w_t} should be of the order of maximum phase acceleration increment over the sampling period.

The measurement dynamic model related to the error state vector can be represented as

$$\mathbf{z}_t = \mathbf{H}\delta\mathbf{x}_t + \mathbf{n}_t, \qquad (25)$$

$\mathbf{z}_t$ is the $m \times 1$ measurement vector at epoch t; $\mathbf{H}$ is the $m \times n$ measurement design matrix; $\mathbf{n}_t$ is zero mean Gaussian measurement noise sequence with covariance, $\mathbf{R}_t$. The single frequency channel carrier phase and frequency measurements related to the error-state vector in the range domain can be written as,

$$\begin{bmatrix} \lambda_k e_{\phi_k} \\ \lambda_k e_{f_k} \end{bmatrix}_t = \begin{bmatrix} 1 & 0 & 0 \\ 0 & 1 & 0 \end{bmatrix} \begin{bmatrix} \delta\rho \\ \delta\dot\rho \\ \delta\ddot\rho \end{bmatrix}_t + \begin{bmatrix} n_{\phi_k} \\ n_{f_k} \end{bmatrix} \lambda_k.$$

For a single frequency channel tracking, $\mathbf{R}_t$ is a 2×2 matrix. $\mathbf{Q}_t$ and $\mathbf{R}_t$ are positive definite matrices (i.e. $\mathbf{Q} \succ 0$, $\mathbf{R} \succ 0$).

The KF requires an initialization of the state vector, $\delta\mathbf{x}_0$, and state error covariance $\mathbf{P}_0$, and an exact knowledge of the process noise covariance $\mathbf{Q}_t$ and measurement noise covariance $\mathbf{R}_t$, based on the prior information of the system and signal operating environment. The steady-state KF gain can be computed as [23],

$$\mathbf{K}_{t+1} = \mathbf{P}_{t+1|t}\mathbf{H}^T(\mathbf{H}\mathbf{P}_{t+1|t}\mathbf{H}^T + \mathbf{R}_{t+1})^{-1}, \qquad (26)$$

$$\mathbf{P}_{t+1|t} = \mathbf{F}\mathbf{P}_{t|t}\mathbf{F}^T + \mathbf{Q}_t, \qquad (27)$$

where $\mathbf{K}_{t+1}$ is the 3×2 Kalman gain matrix at epoch $t+1$.

The error-state KF equations can be written as

$$\delta\hat{\mathbf{x}}_{t+1|t} = \mathbf{F}\delta\hat{\mathbf{x}}_{t|t}, \qquad (28)$$

$$\delta\hat{\mathbf{x}}_{t+1|t+1} = \delta\hat{\mathbf{x}}_{t+1|t} + \mathbf{K}_{t+1}\tilde{\mathbf{z}}_{t+1}, \qquad (29)$$

$$\tilde{\mathbf{z}}_{t+1} = \mathbf{z}_{t+1} - \mathbf{H}\delta\hat{\mathbf{x}}_{t+1|t}, \qquad (30)$$

with $\tilde{\mathbf{z}}_{t+1}$ the innovation of the measurement vector, which is used to update the predicted state vector, $\delta\hat{\mathbf{x}}_{t+1|t}$, and $\mathbf{P}_{t+1|t}$ is the prediction error covariance matrix.

The multiple-frequency signal dynamic tracking KF state-vector can be initialized with a prior estimate of phase and frequency errors, which are estimated within the STL, as,

$$\delta\hat{\mathbf{x}}_0 = \begin{bmatrix} \delta\rho \\ \delta\dot\rho \\ \delta\ddot\rho \end{bmatrix} = \begin{bmatrix} \delta\phi_k \\ \delta f_{D_k} \\ \delta\dot f_{D_k} \end{bmatrix} \lambda_k. \qquad (31)$$

The KF error-state estimate $\delta\hat{\mathbf{X}}_{t+1}$ is conditioned on knowing the true values of the system parameters $\mathbf{F}, \mathbf{P}, \mathbf{H}, \mathbf{Q}_t$ and $\mathbf{R}_t$. The time-varying KF gain value is initially influenced by the initial conditions, but eventually ignores them, paying much attention to the process noise and measurement noise covariance matrices. Even then, the assumed noise statistics $\mathbf{Q}_t$ and $\mathbf{R}_t$ are not unconditionally valid for GNSS signal tracking in time-varying signal environments such as ionosphere scintillation, blockage and interference. Hence, in the signal tracking KF, the process noise and measurement errors must be estimated from the measurements. This process leads to tuning the KF using statistical estimation of $\mathbf{Q}_t$ and $\mathbf{R}_t$ values based on the measurements [24], [25]. The AKF is a suitable method for dynamically adjusting the parameters of the KF. There are many approaches for tuning the AKF as summarized in [26]. An innovation-based adaptive estimation is used as the most suitable technique in multiple sensor fusion applications [24] and [25], which is used in this paper for common signal dynamics tracking based on the multiple frequency signal carrier phase error measurements. The idea of an innovation-based AKF is to regularly estimate measurement and process noise covariances using instant carrier phase error measurements. An approach to process multi-frequency channel measurements using AKF in time-varying GNSS signal environment is discussed in the following section.

B. Multi-frequency channel measurement processing

In real GNSS signal environments, multiple frequency signals are subject to either concurrent or non-concurrent frequency selective interference. To track the signal dynamics in such interference signal scenarios, carrier phase and frequency error measurements from multiple frequency channels can be processed in two different ways within the centralized carrier dynamics tracking KF. Namely,

1) Concurrent frequency selective interference occurs in urban canyon and foliage, where the satellite will be shadowed for a short duration, that causes all frequency signals are attenuated or blocked at the same time. In this case, it is beneficial to combine multiple frequency channel measurements in an optimal way to obtain a minimum mean square error (MMSE) estimate of the common geometric Doppler frequency error between the received and reference signals. This approach will reduce the influence of interference in each frequency channel measurement by means of a KF gain distribution. The measurement vector in this case can be represented as a vector of measurements from N multiple frequency channels,

$$\mathbf{z} = \begin{bmatrix} \mathbf{z}_1, \cdots, \mathbf{z}_N \end{bmatrix}, \qquad (32)$$

This approach has limitations to be used in non-concurrent interference scenarios, due to the propagation of errors from weak signal tracking loops to strong signal tracking loops.

2) Non-concurrent frequency selective interference is most likely due to intentional or unintentional RF interference such as multipath, jamming and spoofing. In such signal conditions, it is beneficial to use measurements from a signal frequency channel that is not under the influence of interference. This approach avoids the propagation of errors from weak signal tracking channels to stronger
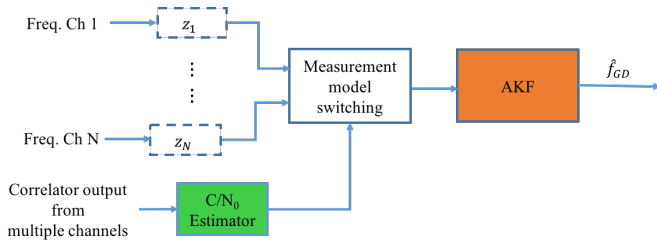
Figure 4: LOS Doppler frequency estimation using an Adaptive Kalman Filter scheme.

signal tracking channels. In non-concurrent interference signal scenario, the measurement vector is chosen from multiple frequency channels based on a maximum carrier-to-noise ratio criteria,

$$\mathbf{z} = \max_{C/N_0} \left[\mathbf{z}_1, \cdots, \mathbf{z}_N \right]. \tag{33}$$

Notice that this approach is not a suitable solution when all the frequency channels are under the influence of interference.

The two signal conditions discussed above will be sensed by using a C/N_0 estimator in each frequency channel, compared to a C/N_0 threshold. In the former case, the optimal value KF gain weighting each frequency channel measurement is computed based on the measurement noise variance. While in the latter case, signal phase and frequency error measurements from the high C/N_0 signal channel will be chosen to estimate the KF error-state vector. To avoid the propagation of errors from weak signal channel measurements to stronger channel measurements, it is necessary to sense and exclude the weak signal channel measurements from the measurement vector. The channel condition is indicated by the C/N_0 estimator to measurement switching block, in order to switch between concurrent and non-concurrent measurement models as shown in Fig. 4.

In time-varying signal environment, a reliable estimation of C/N_0 level of each channel is necessary to enable the dynamic operation of CTL. In general, the C/N_0 estimation in weak signal environments is biased from the truth. An unbiased estimate of the C/N_0 level in weak signal environments can be obtained by increasing the coherent integration time as shown in [27]. The more detailed information on the C/N_0 estimation techniques in GNSS receiver can found in [27] and [28]. The estimated C/N_0 level in each channel is compared to C/N_0 threshold in order to switch the measurement models in CTL. The criteria to fix C/N_0 threshold in CTL can be obtained through simulations and the C/N_0 tracking threshold performance of multiple frequency signals in standard carrier tracking loop architecture.

The carrier phase and frequency error measurements from multiple frequency channels in the phase domain will be transformed to range domain to estimate range and range error rate using the KF. The KF error-state vector which includes range error, range error rate and range acceleration error needs to be transformed back to the phase domain by appropriate scaling with the inverse of the signal wavelength, to obtain the corresponding geometric Doppler frequency in each frequency channel, and then be used to tune the corresponding carrier NCO,

$$\delta f_{GD_k} = \left(\frac{1}{\lambda_k} \right) \delta \dot{\rho} \tag{34}$$

The estimation process of measurement and process noise covariances in AKF using instant carrier phase error measurements is discussed in the following section.

C. Estimation of measurement and process noise covariances

The essential step in the innovation-based AKF is the estimation of the innovation covariance. The covariance of the innovation sequence can be estimated using a simple moving average filter as given in [20],

$$\hat{\mathbf{C}}_{\tilde{\mathbf{z}}_t} = \frac{1}{M} \sum_{j=t-M+1}^{t} \tilde{\mathbf{z}}_j \tilde{\mathbf{z}}_j^T \tag{35}$$

where $\tilde{\mathbf{z}}_t$ is the measurement innovation sequence; M is the number of samples in the window. The innovation covariance can be estimated from the measurement noise covariance as,

$$\hat{\mathbf{C}}_{\tilde{\mathbf{z}}_t} = \left[\mathbf{H}\mathbf{P}_{t|t-1}\mathbf{H}^T + \mathbf{R}_t \right] \tag{36}$$

In strong signal conditions, the measurement noise variance in GNSS receiver can be obtained from the C/N_0 estimator in each frequency channel carrier tracking loop, as given in [16],

$$\sigma_{e_{\phi_k}}^2 = \left(\frac{1}{4\pi^2 (C/N_0)_k T} \right) \left(1 + \frac{1}{2\pi (C/N_0)_k T} \right) \; [cycles^2] \tag{37}$$

$$\sigma_{e_{f_k}}^2 = \frac{2\sigma_{e_{\phi_k}}^2}{T^2} \; [cycles^2/sec^2] \tag{38}$$

While in degraded signal propagation scenarios, an alternative way to estimate the measurement variance is using a covariance matching approach. From the KF linear measurement model given in (24), the measurement noise at epoch t can be obtained as,

$$\tilde{\mathbf{z}}_t = \mathbf{z}_t - \mathbf{H}\delta\hat{\mathbf{x}}_{t|t-1} \tag{39}$$

By using M noise samples, the unbiased estimator of the measurement covariance $\mathbf{R}$ can be obtained as [29],

$$\hat{\mathbf{R}}_t = \frac{1}{M-1} \sum_{j=t-M+1}^{t} \left((\tilde{\mathbf{z}}_j - \hat{\mathbf{n}})(\tilde{\mathbf{z}}_j - \hat{\mathbf{n}})^T - \frac{M-1}{M}\gamma_t \right) \tag{40}$$

$$\gamma_t = \mathbf{H}\mathbf{P}_{t|t-1}\mathbf{H}^T \tag{41}$$

In case of time-varying measurement noise covariance, a recursive estimation of $\mathbf{R}_t$ from L_r measurement samples can be implemented as

$$\hat{\mathbf{n}}_t = \hat{\mathbf{n}}_{t-1} + \frac{1}{L_r}\left(\tilde{\mathbf{z}}_t - \tilde{\mathbf{z}}_{t-L_r}\right) \tag{42}$$

$$\hat{\mathbf{R}}_t = \hat{\mathbf{R}}_{t-1} + \frac{1}{L_r}\left(\left(\tilde{\mathbf{z}}_t - \hat{\mathbf{n}}_t\right)\left(\tilde{\mathbf{z}}_t - \hat{\mathbf{n}}_t\right)^T\right.$$
$$\left. - \left(\tilde{\mathbf{z}}_{t-L_r} - \hat{\mathbf{n}}_t\right)\left(\tilde{\mathbf{z}}_{t-L_r} - \hat{\mathbf{n}}_t\right)^T\right)$$
$$+ \frac{1}{L_r}\left(\left(\tilde{\mathbf{z}}_t - \tilde{\mathbf{z}}_{t-L_r}\right)\left(\tilde{\mathbf{z}}_t - \tilde{\mathbf{z}}_{t-L_r}\right)^T\right)$$
$$+ \frac{L_r - 1}{L_r}\left(\boldsymbol{\gamma}_{t-L_r} - \boldsymbol{\gamma}_t\right). \tag{43}$$

The measurement noise covariance matrix for N independent multiple frequency channel carrier phase and frequency error measurements can be represented as a diagonal matrix, $\hat{\mathbf{R}}_t = \operatorname{diag}(\sigma^2_{e_{\phi_1}}, \sigma^2_{e_{f_1}}, \cdots, \sigma^2_{e_{\phi_N}}, \sigma^2_{e_{f_N}})$. Similarly, the signal dynamics information which is the process noise covariance $\mathbf{Q_t}$ can be obtained using Doppler frequency rate measurements $\dot{f}_{D_k}$ in each frequency channel. A simple phase acceleration process noise variance estimation using a moving average estimator within a specified window is [30],

$$q_t = \frac{1}{M-1}\sum_{j=t-M+1}^{t}\left[\dot{f}_{D_k}(j) - \frac{1}{M}\sum_{j=t-M+1}^{t}\left[\dot{f}_{D_k}(j)\right]\right]^2 \tag{44}$$

where the units of q_t are [cycles^2/s^4]; $\dot{f}_{D_k}(j)$ represents the signal phase acceleration or frequency rate measurement in [cycles/s^2] obtained from the difference of consequent Doppler frequency outputs in the signal carrier tracking loop. The process noise covariance $\mathbf{Q}_t$ can be estimated by substituting q_t in (24). The estimated values of $\mathbf{R}_t$ and $\mathbf{Q}_t$ can be used to calculate the time-varying optimal value of the KF gain in response to signal dynamics.

However, the simultaneous update of $\mathbf{R}_t$ and $\mathbf{Q}_t$ is not a viable solution as they negatively affect the filter response. Hence, it is reasonable to estimate and update the measurement noise and process noise covariance alternatively in the Kalman gain estimation [26].

D. Kalman filter gain adaption to measurement error variance and signal dynamics

In the centralized dynamics tracking loop filter, carrier phase discriminator output measurements from multiple frequency channels will be combined statistically in an optimal way to obtain the best possible estimate of $\delta\mathbf{x}_t$ based on the time-varying estimates of $\mathbf{Q}_t, \mathbf{R}_t$ and $\mathbf{K}_t$ values. The process noise covariance $\mathbf{Q}_t$ represents the rate of change of the state, while the measurement noise covariance $\mathbf{R}_t$ represents the accuracy of the signal measurements. The optimal weight to multiple signal carrier phase measurements depends on individual signal measurement noise variance $\mathbf{R}_t$ and manifestation of the KF gain. The Kalman gain can be represented in terms of estimated innovation covariance and $\mathbf{Q}_t$ as,

$$\mathbf{K}_t = (\mathbf{F}\mathbf{P}_{t|t-1}\mathbf{F}^T + \mathbf{Q}_t)\mathbf{H}^T\hat{\mathbf{C}}_{\tilde{\mathbf{z}}_t}^{-1}. \tag{45}$$

Then, the KF gain will be manifested based on the carrier phase measurement noise variance and signal Doppler rate as discussed earlier. The KF equivalent noise bandwidth is characterized in comparison to conventional PLL loop filter in [31], [32]. The steady-state KF equivalent noise bandwidth can be computed from the Kalman gain, which is a function of tuning parameters $\mathbf{Q}$ and $\mathbf{R}$ as given in [30],

$$B_{eq} = \frac{\mathbf{K}(\mathbf{Q}, \mathbf{R})}{c_n T} \quad \text{[Hz]} \tag{46}$$

where c_n is the filter coefficient for the n-th order PLL and T is the coherent integration time.

For a third order loop filter, $c_n = 3.048$ and the steady-state gain matrix $\mathbf{K}$ is directly proportional to $\mathbf{Q}$ and inversely proportional to $\mathbf{R}$. This relation enables to construct an adaptive filter bandwidth for time-varying signal environments. In weak signal environments, measurement noise variance $\mathbf{R}$ increases, which in turn reduces the Kalman gain. In high dynamic signal environments, the process noise increases, as a result the Kalman gain tends to increase proportionally. The Kalman filter equivalent bandwidth changes proportional to the gain variation in high dynamic and weak signal conditions.

To evaluate the Kalman filter gain adaption in response to the changing signal power levels and dynamics, we assume that the initial values of noise statistics within the KF are, $\mathbf{P}_0(1,1) = 0.5^2, \mathbf{P}_0(2,2) = 100^2, \mathbf{P}_0(3,3) = 10^2$, process noise tuning parameter is set as, $q = 1$ (cycles^2/s^4), the carrier phase error measurement variance $\sigma^2_{e_{\phi_1}} = 0.05^2$ and $T = 0.02s$.

The time-varying optimal Kalman gain value and the equivalent noise bandwidth in case of signal tracking KF using single frequency channel phase measurement (i.e. non-concurrent frequency selective interference case) at fixed values of $\mathbf{Q}$ and $\mathbf{R}$ is shown in Fig. 5. The Kalman gain value is initially influenced by the state transition covariance to measurement noise ratio, while the Kalman gain steady-state value varies in response to the process noise covariance and measurement noise covariance ratio. In the initial phase of filter operation, the equivalent noise bandwidth is wide enough to cater for the large values of carrier phase and frequency errors and gradually reduced to the steady-state fixed bandwidth value. The transient response of the Kalman filter is controlled by the process noise covariance matrix $\mathbf{Q}$. The KF acts as a fixed bandwidth filter in the steady-state for fixed values of $\mathbf{Q}$ and $\mathbf{R}$.

In case of signal dynamics tracking using combination of two frequency signal measurements (i.e. concurrent frequency selective interference scenario), Kalman filter gain coefficients are adjusted to give weighting to two frequency channel measurements based on individual signal measurement noise variance. For instance, we assume two frequency signal carrier phase error variance is equal, $\sigma^2_{e_{\phi_1}} = \sigma^2_{e_{\phi_2}} = 0.05^2$ cycles^2, hence, the Kalman gain coefficients $\mathbf{K}(1,1)$ and $\mathbf{K}(1,2)$ are equal to process two frequency channel measurements with equal weighting. The KF equivalent noise bandwidth to each of two frequency channel tracking is reduced to half in comparison to single frequency channel tracking as shown in the lower panel of Fig. 6. The reduced bandwidth in each
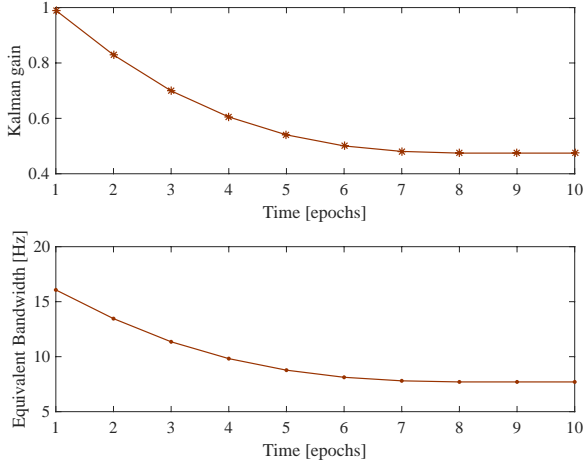
Figure 5: Discrete-time Kalman gain and equivalent noise bandwidth variation in single frequency carrier phase measurement at fixed values of noise statistics.

frequency channel in turn reduces the requirement of C/N_0 tracking threshold and tolerance to in-band RF interference.
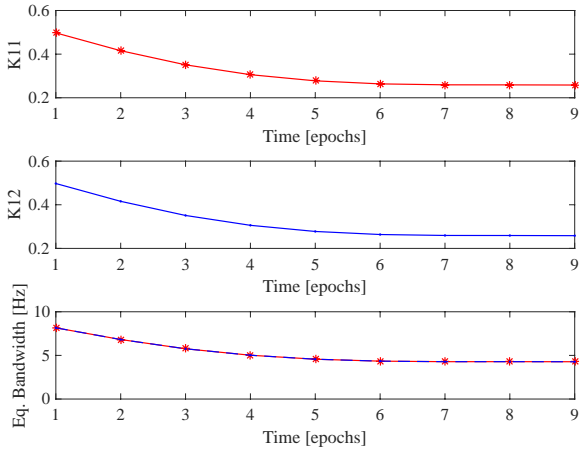

Figure 6: Discrete time Kalman gain values and equivalent noise bandwidth in two frequency channel carrier phase measurements at a fixed values of noise statistics.

Now the KF gain adaption to the changes in signal dynamics and measurement noise variance in two frequency channel tracking is analyzed. The two frequency signals received from the same satellite are subjected to common LOS signal dynamics, but the C/N_0 level in each channel may differ depending on the influence of RF channel effects. As an example, the C/N_0 level is assumed to be varying differently in two frequency channels in three regions (i.e.,'a', 'b' and 'c') as shown in Fig. 7. While the common LOS signal dynamics variation in two-frequency channels is represented by the process noise tuning parameter switching between $q = 0.1$ and 1 (cycles^2/s^4) to represent the low and high signal dynamics scenario respectively. The KF gain coefficients are adapted proportional to two frequency signal carrier phase error mea-

surement statistics (i.e., C/N_0) as shown in Fig. 8. In region 'a', the C/N_0 level set at 45 dB-Hz in first signal is higher than that of second signal C/N_0 level set at 10 dB-Hz. The two frequency channel measurement noise variance is calculated based on C/N_0 values and Kalman gain values are updated to offer high gain to the first frequency channel measurements in region 'a', while the second frequency channel measurements are excluded from the measurement vector as shown in Fig. 8. The KF gain in the steady state is changing with respect to the signal process noise covariance, i.e., $q = 0.1$ and 1 (cycles^2/s^4).
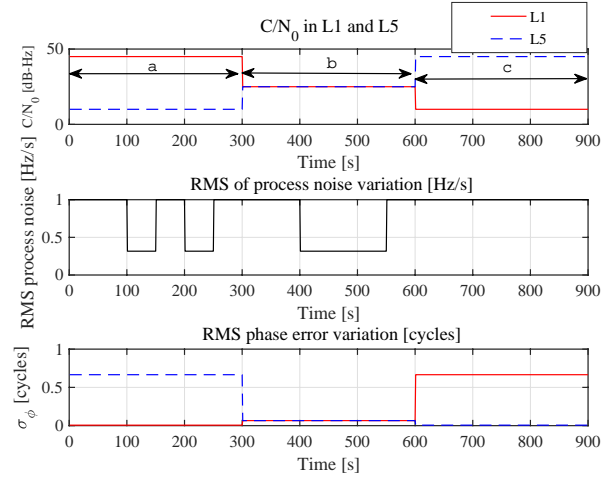

Figure 7: Signal power levels and dynamics variation in received two frequency signals.

In region 'b', C/N_0 level in two frequency channels is reduced to 25 dB-Hz, which is the concurrent frequency selective interference scenario. The Kalman gain value in region 'b' is equally distributed to process two frequency channel measurements. At higher signal dynamics, i.e., $q = 1$
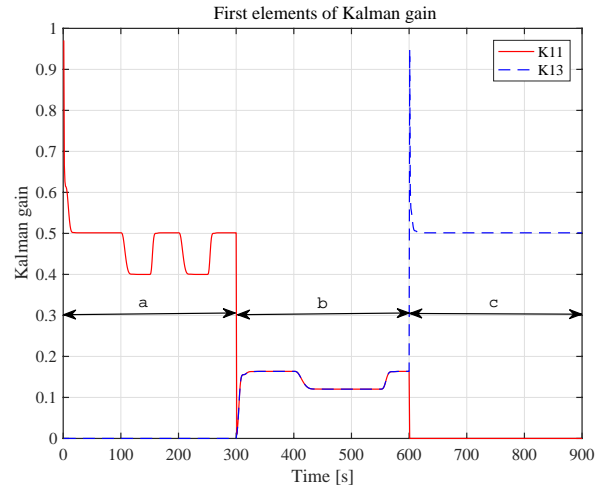

Figure 8: Discrete Kalman gain adaption in AKF to measurement noise and process noise variance of two frequency signals.
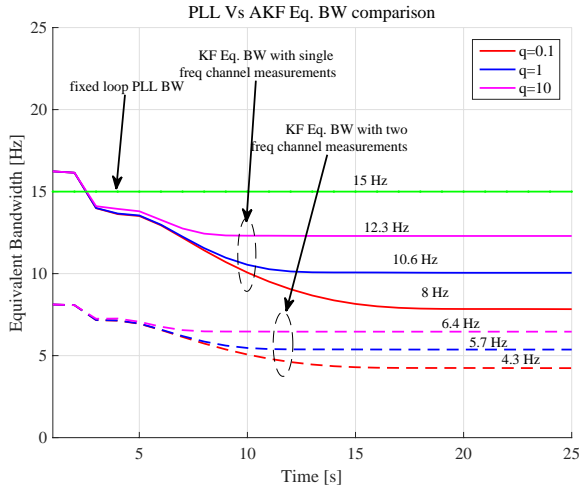
Figure 9: Comparison of Equivalent Bandwidth in fixed BW PLL Loop filter and AKF using single and two frequency channel measurements at C/N0 of 50 dB-Hz

Figure 10: PLL error in L1 and L5 signal carrier tracking loop at q=1, using AKF with single and dual frequency signal phase observations in reference to fixed loop BW PLL.

(cycles^2/s^4), KF gain values are indeed high even at low C/N_0 values to respond to the changes in carrier frequency deviation. In region 'c', first channel C/N_0 value is significantly lower than that of second channel. The KF gain is high for the second signal measurements in region 'c' and the first frequency channel measurements are excluded from the estimation process.

IV. PERFORMANCE ANALYSIS OF CENTRALIZED MULTI-FREQUENCY DYNAMICS TRACKING LOOP

To evaluate the performance benefits of the proposed adaptive CTL tracking loop, a simple analysis of KF equivalent bandwidth using single and two-frequency signal measurements is shown with reference to standard PLL fixed loop bandwidth in Fig. 9. The Kalman filter equivalent bandwidth is computed as per the relation given in (46) [30] for three different signal dynamic profiles, i.e. $q = 0.1, 1$ and 10 (cycles^2/s^4) at a C/N_0 of 50 dB-Hz in each frequency channel.

In CTL, either a single or combination of multiple frequency channel phase measurements is utilized to estimate the signal dynamics using AKF. In AKF, the time-varying KF gain and the equivalent bandwidth are adapted to the changing signal dynamics and to the measurement noise sequentially as discussed earlier. In frequency-selective interference scenario, where one or more number of frequency channels are under the influence of interference, combining multiple frequency channel measurements causes the propagation of errors from weak signal channels to the strong signal channel tracking loop. In such a case, it is beneficial to use the relatively stronger signal channel measurements to estimate the LOS signal dynamics. In case of concurrent interference scenario, where all the frequency channels are under the influence of fading or attenuation, it is beneficial to use the optimal weighted combination of multiple frequency channel measurements to estimate LOS signal dynamics. In the concurrent interference, Kalman filter gain is distributed to give appropriate weights to all the available frequency channel
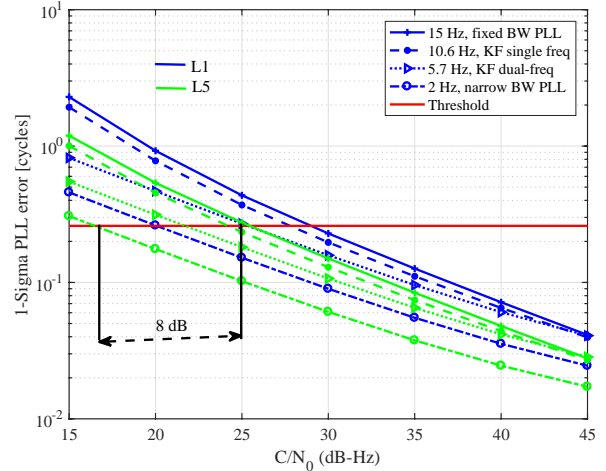
measurements based on respective signal measurement noise statistics. The equivalent noise bandwidth in each frequency channel tracking loop is adapted proportionally to the Kalman gain distribution across multiple channel measurements. The reduced tracking loop bandwidth in each frequency channel reduces the requirement of C/N_0 tracking threshold. The reduced C/N_0 tracking threshold, in turn, increases the signal tracking loop tolerance to RF interference [33]. As a result, the influence of interference on each frequency channel reduces proportionally to the Kalman filter bandwidth.

As an example, 1-sigma value of carrier-phase noise in GPS L1 and L5 signal tracking loop using AKF with single and dual-frequency channel measurements is evaluated using analytical error models [16], as shown in Fig. 10, at $q = 1$ (cycles^2/s^4).

The steady-state value of the KF equivalent bandwidth using single and dual-frequency channel measurements is 10.6 Hz and 5.7 Hz respectively at a process noise variance of $q = 1$ (cycles^2/s^4), as shown in Fig. 9. The single frequency channel KF tracking loop has the benefit of 2 dB tracking threshold and the dual-channel KF loop has a benefit of 4 dB tracking threshold in each channel in comparison to the 15 Hz fixed loop bandwidth PLL. In the case of non-concurrent frequency selective interference scenario, where the signal dynamics are estimated using a relatively stronger channel phase measurements and all the other frequency channels tracked using second-order PLL of 2 Hz BW, have a benefit of 8 dB improvement in C/N_0 tracking threshold. As a result, the narrow loop bandwidth signal tracking with LOS signal dynamics aided from CTL has reduced the C/N_0 tracking threshold requirement of 29/25 dB-Hz in STL to 21/17 dB-Hz for L1/L5 signals respectively. This in turn increases the robustness to intentional and unintentional interference in each frequency channel.

The multiple frequency signals transmitted at different radio frequency in the L-band spectrum are influenced differently by the intentional and unintentional RF interference. A character-

ization of GPS receiver performance during RF interference [34] and ionosphere scintillation is studied in [35], [36]. When the interference signal enters the receiver along with the intended signal, effective carrier to noise power changes [34] as,

$$(C/N_0)_{eff} = \frac{1}{\frac{1}{C/N_0} + \frac{J/C}{Q_J R_c}} \qquad (47)$$

where C/N_0 is the unjammed carrier-to-noise ratio; J/C is the jammer-to-signal carrier power ratio; Q_J is a jamming-resistance quality factor; R_c code rate of the PRN code. Typical value of Q_J is 1 for single tone continuous wave (CW) interference, 1.5 for matched spectrum (MS) and 2.2 for band-limited white noise (BLWN) spectrum [16]. An increased value of $Q_J R_c$ factor in (47) results in an increased jamming resistance in the receiver. The GPS L5 and GALILEO E5 signals with 10 times higher chip rate and more received power than GPS L1 have the benefit of higher value of $Q_J R_c$ factor, and are more immune to RF interference than other frequency signals in GPS and GALILEO. However, when multiple frequency channels are processed by the equal receiver front end bandwidths, the influence of broadband noise jammer is equal on all signals and in-creased code chipping rates do not improve the immunity.

Ionospheric scintillation is an unintentional RF interference to the GNSS receiver. Ionospheric scintillations near the poles and the equator adversely affects the operation of a receivers PLL and leads to carrier cycle slips, navigation data bit errors, and complete loss of carrier lock [37]. After GNSS modernization, the influence of ionosphere scintillation at L1, L2, and L5 frequency bands is characterized by [38]. The GPS L1, L2, and L5 signal tracking performance during scintillation is assessed by analyzing the experimental data collected during the solar maximum period in [39]. These studies have concluded that the low carrier frequency signals, L2C and L5 tracking is less robust to scintillation than GPS L1 signal, despite the advanced signal characteristics such as high chip rate and power.

In the light of the above discussion, the diversity in the performance of multi-frequency GNSS signals can be best utilized by employing the proposed CTL architecture in GNSS receiver to complement each other in challenging signal environment such as blocking, jamming/spoofing and ionosphere scintillation.

The performance benefits of the proposed CTL architecture are summarized as follows:

- **Computational efficiency:** The replacement of a multiple number of higher order carrier tracking loops by a single centralized dynamics tracking filter and multiple narrow bandwidth PLLs improves the computational efficiency of the GNSS receiver significantly, which in turn is a power-efficient solution.
- **Restoration of temporary loss-of-lock:** During the receiver operation in real GNSS signal environment, the signal tracking loop may lose lock for a short time interval when the frequency channel is being shadowed or blocked. In such a case, it is necessary to reacquire the signal to resume signal tracking process after the

signal reappears. The signal re-acquisition is a computationally intensive process in scalar tracking loops. In the proposed centralized dynamics multi-frequency tracking architecture, a LOS Doppler shift aid is provided by the CTL to all the frequency channels, including the blocked channels to restore the lost tracking process after the signal reappears. This, in turn, eliminates the need of re-acquisition process.

- **Robustness to Interference:** In multi-frequency CTL architecture, individual frequency signal tracking using narrow bandwidth PLL assisted by LOS Doppler frequency information from AKF is inherently less sensitive to interference than the standard tracking loop. Hence, the frequency selective interference such as jamming or spoofing on CTL needs higher jamming power to that of STL to disrupt the intended frequency channel tracking process.
- **Robustness to Spoofing:** The CTL provides the LOS signal dynamics aid to the narrow-band tracking loop in each frequency channel. The influence of a spoofing signal with dynamics deviated from the authentic signal on selective frequency channels can be detected and rejected due to the mismatch between the received spoofing signal dynamics and authentic signal dynamics aided by the CTL. At most, the frequency selective spoofing impairs the targeted frequency channel from tracking the legitimate signal and leads to a jammed state. Therefore, the false signal can never be tracked by any of the spoofed channels while the authentic signal dynamics are provided by the CTL. Hence, the CTL architecture improves the receiver robustness to frequency selective spoofing by making use of redundancy of a number of frequency signals.
- **Improvement in position accuracy:** The common Doppler-aided multi-frequency channel tracking using CTL will result in common mode observation errors in multiple channels. The common-mode observations errors tend to cancel out when a linear combination of the observations are generated, such as ionosphere-free, wide-lane etc. as shown in [19]. This, in turn, leads to improvement in position accuracy and precision.

V. EXPERIMENTAL RESULTS

The proposed centralized-dynamics tracking-loop architecture for multiple-frequency signals is evaluated through experiments using live satellite data collected from Block-IIF satellite constellation. A COTS (commercial off-the-shelf) based wide-band RF front-end SDRNav40 with 20.46 MHz pre-correlation bandwidth and 27.456 MHz sampling rate was used to collect L1 C/A and L5 signal data. Digitized IF data from the RF front-end was processed in a multi-frequency software receiver, which has been tailored for this project based on [40]. The standard carrier tracking loop was designed with an FLL-assisted third order PLL for multiple frequency channels with 15 Hz PLL loop filter BW and 10 Hz FLL BW. The CTL architecture was realized using one common dynamics tracking adaptive Kalman filter and multiple narrow
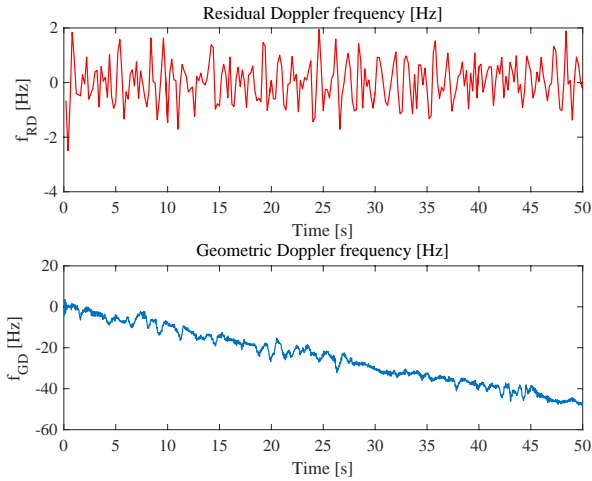
Figure 11: Geometric Doppler and residual Doppler variation of received signal in static case in L1 tracking loop using CTL.

Figure 12: Test set up for Jamming attack

bandwidth second order closed loop PLLs are employed. The loop bandwidth required to track residual phase variations in each frequency channel was obtained from a prior estimation of residual signal phase variations through experimental data.

It is to be noted that received signals with C/N_0 below 30 dB-Hz are considered as weak signals, while signals in the C/N_0 above 30 dB-Hz are considered as stronger signals based on the simulations. Hence, the measurement model switching in KF is based on the C/N_0 threshold of 30 dB-Hz for the experimental evaluation of CTL. The C/N_0 level in each frequency channel is estimated using sliding window of correlation output samples and narrow-to-wideband power ratio method with an integration time of 1 s. In strong signal conditions, the R-matrix in AKF is obtained from the C/N_0 estimator. While in weak signal conditions, R-matrix is estimated using an alternative approach mentioned in Section III-C. In weak signal conditions, KF gain estimation is not dependent on the C/N_0 level estimation accuracy error.

From the experimental results shown in Fig. 11, the residual Doppler frequency variation in each frequency channel is within the range of 2 Hz. Hence, the closed-loop PLL in each frequency channel was realized using second order PLL with 2 Hz loop bandwidth to track residual phase variations specific to each frequency channel. The centralized dynamic tracking filter was realized using third-order adaptive Kalman filter. The initial noise statistics of Kalman filter are assumed in phase domain as, $\mathbf{P}_0(1,1) = 0.5^2, \mathbf{P}_0(2,2) = 100^2, \mathbf{P}_0(3,3) = 10^2$. The process acceleration noise variance and measurement noise variance is estimated from the STL tracking loop results. The geometric Doppler variation has a slope of 1 Hz/s as shown in Fig. 11, hence, reasonable value $q = 1$ (cycles^2/s^4) and phase measurement noise variance in L1 is $\sigma_{e_{\phi_1}}^2 = 0.02^2$ (cycles^2) and in L5, $\sigma_{e_{\phi_1}}^2 = 0.01^2$ (cycles^2).

As GNSS signals being spread spectrum in nature are inherently more immune to conventional jamming waveforms such as CW, Pulse signal etc. As a result conventional jamming waveforms needs hig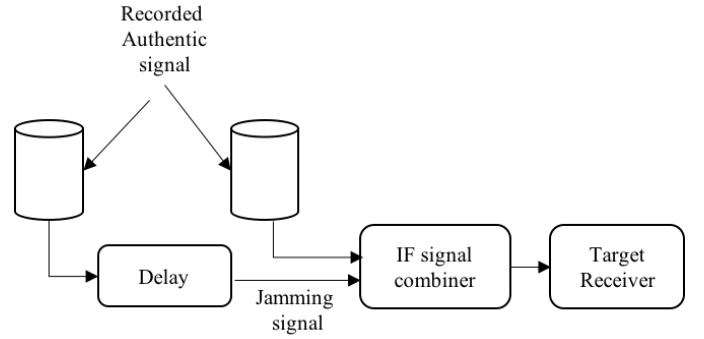her power that is beyond the thermal noise level to disrupt the receiver functionality. Moreover, with advanced receiver technology, any interference signal with power level beyond the GNSS signal dynamic range can be easily detected by an automatic gain control mechanism in the RF Front and be limited before entering to the signal processing stage of a receiver. Hence, an interference signal which can not be detected at the front-end and reach out to the processing stage of a GNSS receiver is matched spectrum jamming waveform. Hence, to evaluate the performance of a proposed centralized multi-frequency dynamic tracking loop, we have considered matched spectrum jamming waveform as a potential source. The matched spectrum jamming waveform is generated using a delayed version of the recorded signal as shown in Fig. 12.

Here, we have demonstrated the performance of CTL in case of concurrent and non-concurrent interference in multiple frequency signals.

- Case 1: Concurrent frequency selective interference: Both L1 and L5 are jammed at J/C of 15 dB at the same time instant.

In this experiment, the LOS signal dynamics tracking using two frequency channel measurements model in CTL is evaluated subjected to RF interference on two-frequency channels at the same time instant. As shown in Fig. 13, both L1 and L5 signal channels are under the influence of matched spectrum jamming at J/C of 15 dB during the time interval $40 - 60s$. The GPS L1 and L5 signal tracking using wideband PLL in STL failed to track during the interference and beyond, which needs re-acquisition of signals. In CTL, the interference in GPS L1 and L5 signal channels is sensed by C/N_0 estimator in each frequency channel and concurrent measurement model is selected to estimate LOS signal dynamics. The Kalman filter gain is distributed across two frequency channel measurements and the equivalent noise bandwidth in each frequency channel is reduced proportional to the KF gain values. As a result, L1 and L5 signal tracking loop has an advantage of C/N_0 tracking threshold of about 3dB compared to STL as shown in the upper panel of Fig. 13. The CTL loop is succeeded in tracking L1 and L5 signals even at J/C of 15 dB.

- Case 2: Non-concurrent frequency selective interference: Both L1 and L5 are jammed at J/C of 12 dB at different time intervals.
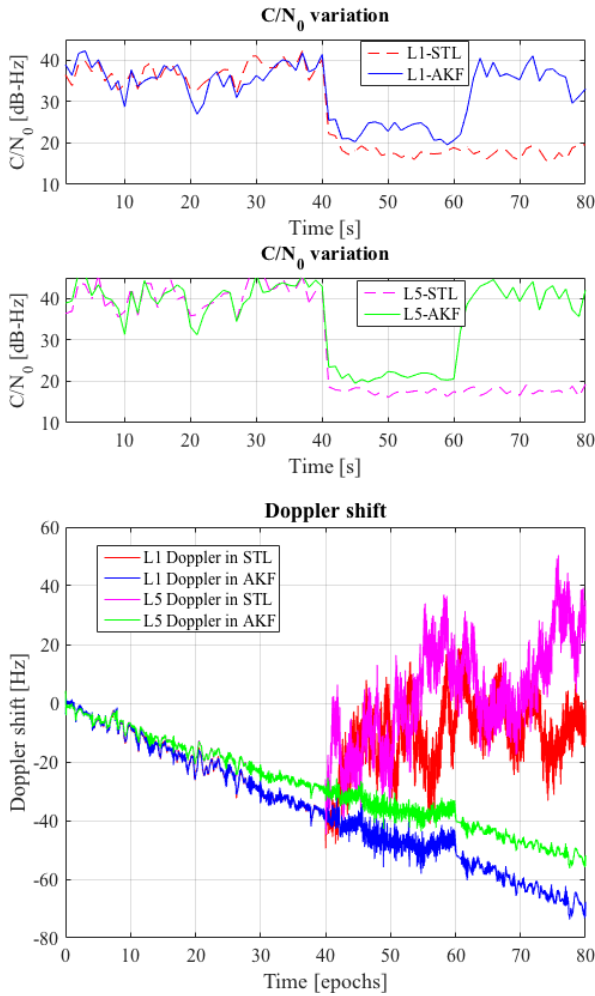
Figure 13: Signal dynamics estimation in the CTL using GPS L1 and L5 signal measurements in concurrent frequency selective interference scenario during the time interval $40 - 60s$.
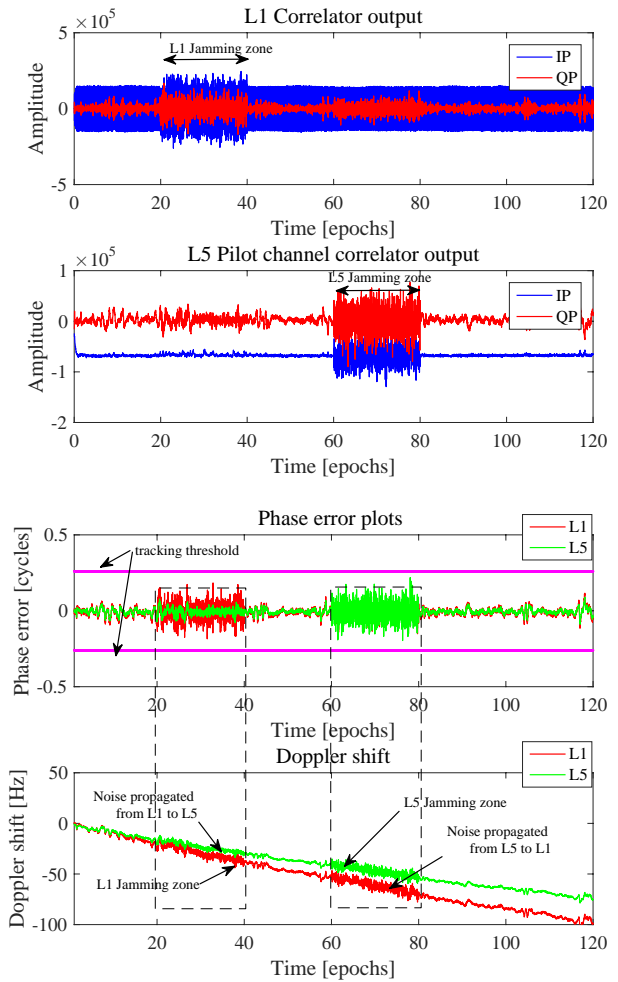

Figure 14: Signal dynamics estimation in the CTL using GPS L1 and L5 signal measurements in non-concurrent frequency selective interference scenario.

In this experiment, the CTL signal tracking using two frequency signal measurements model is evaluated subjected to frequency selective interference on two-frequency channels at different time intervals. During $1 - 20s$ and $40 - 60s$ time intervals, both GPS L1 and L5 signals have high C/N_0 levels, hence, the combined signal measurement tracking do not degrade the signal dynamics estimation within the CTL. During the $20 - 40s$ time interval, GPS L1 is under the influence of interference, while L5 is not.

During the jamming period, GPS L1 signal C/N_0 is degraded, which in turn has increased L1 carrier phase measurement error as shown in Fig. 14. The CTL gain coefficients are adapted to changes in two frequency signal measurements, proportionally L1 measurements are given low weighting, but not excluded from the signal dynamic estimation process. During $60 - 80s$ time interval, the L5 signal is jammed, while L1 is not. The Kalman gain coefficients are adapted to process L1 signal measurements with a high gain and L5 phase measurements with a low gain. As a result, in both cases, the CTL correctly estimates the geometric Doppler shift information, which is provided to closed loop PLL tracking

loops in each frequency channel. The carrier phase error in L1 and L5 tracking loops are below the tracking threshold of 0.26 cycles. Then the tracking loop continued to track L1 and L5 signals at J/C of 12 dB. However, the combined signal measurement based signal dynamics estimation propagated errors from weak signal tracking loop to stronger signal tracking loop as shown in lower panel of Fig. 14.

The first elements of the Kalman gain coefficient adaption to L1 and L5 signal measurement noise is shown in Fig. 15

• Case 3: Non-concurrent frequency selective interference: L1 is jammed using J/C of 15 dB, while L5 not.

The performance of L1 and L5 signal tracking using the STL and CTL using single measurement model is evaluated during L1 jamming at J/C of 15 dB as shown in Fig. 16.

Under the influence of interference, L1 signal C/N_0 degradation using the STL is about 7 dB more compared to the CTL signal tracking loop. In the CTL, L1 signal is tracked using 2 Hz loop bandwidth PLL assisted by signal dynamics information from the CTL estimated using L5 phase measurements. The narrow bandwidth PLL tracking in L1 frequency channel improved the tracking threshold and resistance to interference,
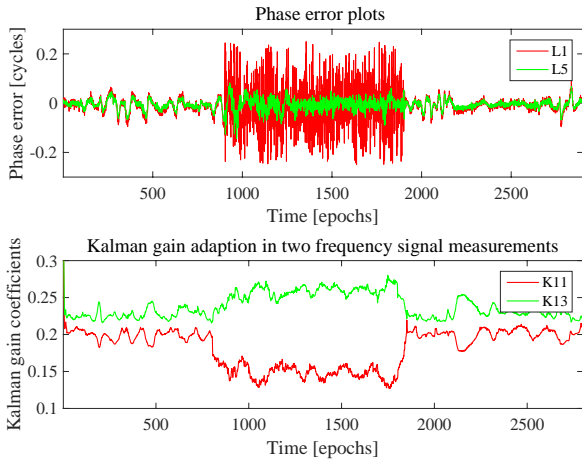
Figure 15: First elements of the CTL gain coefficients in response to two frequency signal carrier phase measurement noise.
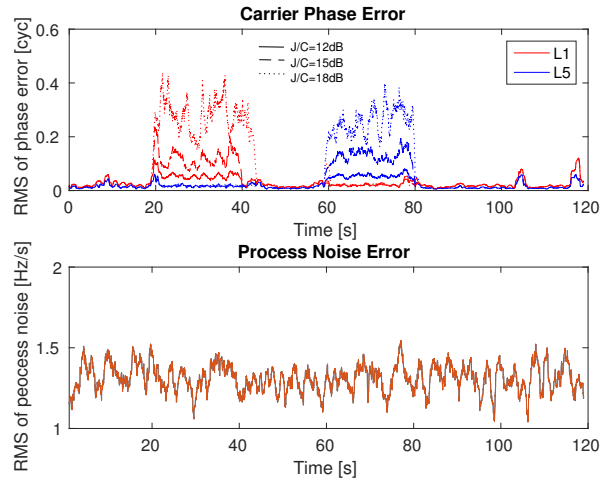

Figure 17: Measurement and process noise on-line error estimation in a frequency selective interference scenario
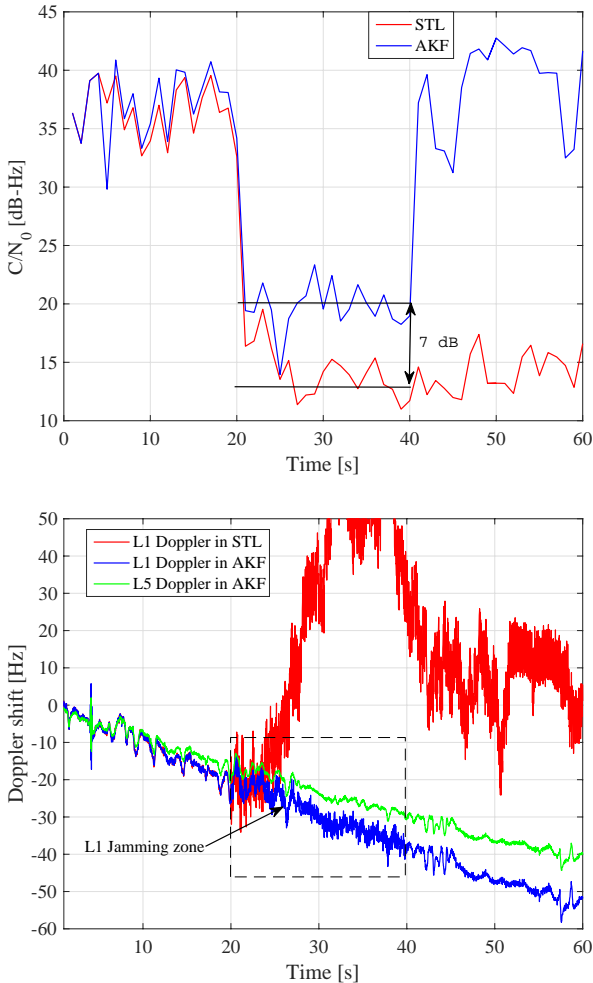

Figure 16: Performance comparison of GPS L1 signal tracking using STL and CTL with single measurement model (a) L1 Carrier to Noise power variation during Jamming period from 20s-30s at J/C of 15dB, (b) L1 and L5 Signal Doppler variation.

i.e. jamming margin. Hence, the impact of interference on the CTL is lower compared to the STL using 15 Hz loop bandwidth. Moreover, there is no propagation of errors from L1 signal tracking loop measurements to L5 signal tracking loop measurements as shown in Fig. 16.

The CTL provides the signal dynamic information to individual frequency channel closed loop PLLs, even to the channels that are under the influence of jamming. The Doppler frequency variation in the jammed L1 frequency channel using both CTL and STL is shown in Fig. 16. In the STL, the jamming caused discontinuity in signal tracking, which needs to reacquire the signal to restore the tracking process. In the CTL, signal dynamics are provided by the AKF to the jammed frequency channel while it is still under jamming. Hence, after the jamming signal being seized from the frequency channel, the tracking process is restored back without any re-acquisition process.

To analyze the phase error and process noise error variation at different J/C power levels, root mean square values of measurement noise and process noise error is estimated on-line using a moving average filter technique as discussed earlier, and is shown in Fig. 17. The estimated values of measurement and process noise variances are used in manifestation of Kalman gain in response to changing signal environment. The GPS L1 tracking loop resistance to jamming is evaluated by varying the jamming power level relative to signal carrier power, as shown in Fig. 18. The narrow bandwidth PLL tracking in each frequency channel improves the tracking threshold and resistance to interference, i.e. increases jamming margin. At J/C of 12 dB, the STL carrier-to-noise ratio has degraded to 20 dB-Hz, below the tracking threshold, which causes the tracking loop failure. While using the CTL, the carrier to noise degradation is lower compared to the STL. The L1 channel tracking in our proposed architecture has improved the C/N_0 tracking threshold by 7 dB in challenging signal environments compared to STL.
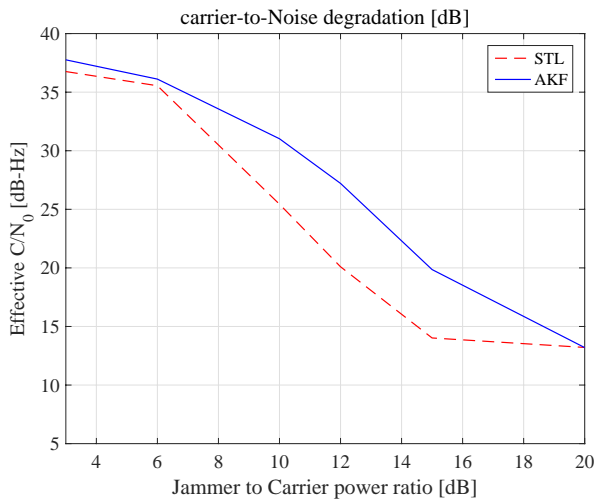
Figure 18: C/N_0 degradation in L1 tracking loop at varying jamming power levels.

VI. CONCLUSIONS

We proposed a centralized multi-frequency dynamics tracking-loop architecture using an adaptive Kalman filter (AKF). The multiple signal carrier tracking using narrow-loop bandwidth PLLs reduce the carrier-phase noise in each frequency channel, while the common signal dynamics estimation using the new centralized dynamic tracking AKF enhances the receiver dynamic performance. The common signal dynamics tracking using AKF based on the optimal combination of multiple carrier-phase error measurements enhanced the individual signal tracking-loop sensitivity and robustness in challenging signal environment such as frequency-selective blocking, jamming, and spoofing. Furthermore, the replacement of multiple number of higher order tracking loops by a single dynamics AKF tracking loop filter and multiple narrow loop bandwidth PLLs increase the computational efficiency in tracking.

REFERENCES

[1] B. C. Kim and M.V. Tinin, "Potentialities of multi-frequency ionospheric correction in global navigation satellite systems," *Journal of Geodesy*, vol. 85, no. 3, pp. 159–169, 2011.

[2] K. Wang and M. Rothacher, "Ambiguity resolution for triple-frequency geometry-free and ionosphere-free combination tested with real data," *Journal of Geodesy*, vol. 85, no. 3, pp. 539–553, 2013.

[3] J. W. Sennott and D. Senffner, "Navigation receiver with coupled signal-tracking channels," *U.S. Patent*, , no. 5343209A, 1994.

[4] J. W. Sennott and D. Senffner, "Robustness of tightly-coupled integrations for real-time centimetre GPS positioning," in *Proc. ION-GPS*, Kansas City, MO, 1997, pp. 655–663, Institute of Navigation.

[5] P. Closas and A. Gusi-Amigó, "Direct Position Estimation of GNSS Receivers: Analyzing main results, architectures, enhancements, and challenges," *IEEE Signal Processing Magazine*, vol. 34, no. 5, pp. 72–84, 2017.

[6] J. J. Spilker, "Vector delay lock loop processing of radiolocation transmitter signals," *U.S. Patent*, vol. 85, no. 5398034, pp. 539–553, 1995.

[7] M. Zhodzishsky, S. Yudanov, V. Veitsel, and J. Ashjaee, "Co-op tracking for carrier phase," in *Proc. ION-GPS*, Nashville, TN, 1998, pp. 653–664, Institute of Navigation.

[8] T. Pany, R. Kaniuth, and B. Eissfeller, "Deep integration of navigation solution and signal processing," in *Proceedings of Institute of Navigation GPS/GNSS Conference*, Long Beach, CA, 2005, pp. 1095 – 1102, Institute of Navigation.

[9] M. Lashely and D. M. Bevly, "Analysis of discriminator based vector tracking algorithms," in *Proceedings of the Institute of Navigation (NTM)*, San Diego, CA, USA, 2007, pp. 570 – 576, Institute of Navigation.

[10] P. Henkel, K. Giger, and C. Gunther, "Multifrequency, multisatellite vector phase-locked loop for robust carrier tracking," *IEEE Journal of Selected Topics in Signal Processing*, vol. 3, no. 4, pp. 674–681, 2009.

[11] P. Senlin, M. Yu, and D. Ruihui, "A multiple-frequency GPS software receiver design based on a vector tracking loop," in *Proceedings of the Institute of Navigation (NTM)*, Myrtle Beach, SC, USA, 2012, pp. 495–505, IEEE.

[12] R. K. Siddakatte, A. Broumandan, and G. Lachapelle, "Enhanced carrier phase tracking in fading environments using frequency diversity," in *European Navigation Conference (ENC)*, Helsinki, Finland, 2016, pp. 1–6, IEEE.

[13] J. Vilà-Valls, P. Closas, and J. T. Curran, "Multi-frequency GNSS robust carrier tracking for ionospheric scintillation mitigation," *Journal of Space Weather and Space Climate*, vol. 7, no. A26, October 2017.

[14] J. A. Klobuchar, "Total ionosphere effects on gps," *GPS World*, April 1991.

[15] S. Alban and D. Gebre-Egziabher, "Performance analysis and architectures for INS-aided GPS tracking loops," in *Proccedings of the ION NTM-03*, Anaheim, CA, 2003, Institute of Navigation.

[16] P. Ward, E. D. Kaplan, and C. J. Hegarty, *Satellite signal acquisition and tracking, in Understanding GPS: Principles and Applications*, Artech House, Boston, 2006.

[17] A. Patapoutian, "On phase-locked loops and Kalman filters," *IEEE Transactions on Communications*, vol. 47, no. 5, pp. 670672, 1999.

[18] J. Vilà-Valls, P. Closas, M. Navarro, and C. Fernández-Prades, "Are PLLs dead? A tutorial on Kalman filter-based techniques for digital carrier synchronization," *IEEE Aerospace and Electronic Systems Magazine*, vol. 32, no. 7, pp. 28–45, 2017.

[19] P. Bolla and E. S. Lohan, "Dual-frequency signal processing architecture for robust and precise positioning applications," in *Proc. of IEEE/ION PLANS*, Monterey, CA, 2018, pp. 72–80, IEEE/ION.

[20] A. H. Jazwinski, "Adaptive filtering," *Journal Automatica*, vol. 5, no. 4, pp. 475–485, 1969.

[21] M. Psiaki and H. Jung, "Extended Kalman filter methods for tracking weak GPS signals," in *Proceedings of the 15th ITM-ION*, Portland, OR, 2002, pp. 2539 – 2553, Institute of Navigation.

[22] Y. Bar-Shalom, X. Rong Li, and T. Kirubarajan, *Estimation with Applications to Tracking and Navigation*, John Willey and Sons, New York, 2001.

[23] R. G. Brown. and P. Y. C. Hwang, *Introduction to Random Signals and Applied Kalman Filtering*, John Willey and Sons, New York, 1997.

[24] A. H. Mohamed and K. P. Schwarz, "Adaptive Kalman filtering for INS/GPS," *Journal of Geodesy*, vol. 73, no. 4, pp. 193203, 1993.

[25] R. K. Mehra, "On the identification of variance and adaptive Kalman filtering," *IEEE Transactions on Automatic Control*, vol. 15, no. 2, pp. 175 – 184, 1970.

[26] M. Shyam Mohan, R. M. O Naren Naik, M. R Gemson, and Ananthasayanam, "Introduction to the kalman filter and tuning its statistics for near optimal estimates and Cramér-Rao bound," Report TR/EE2015/401, IIT Kanpur, 2015.

[27] P. D. Groves, "Gps signal to noise measurement in weak signal and high interference environments," in *Proc. of the 18th International Technical Meeting of the Satellite Division of The Institute of Navigation*, Long Beach, CA, 2005, p. 643658, ION.

[28] K. Muthuraman and D. Borio, "C/N0 estimation for modernized GNSS signals: Theoretical bounds and a novel iterative estimator," *Navigation*, vol. 57, no. 4, pp. 309–323, 2010.

[29] J. Vilà-Valls, P. Closas, Carles Fernndez-Prades, and Javier Arribas, "Noise statistics estimation techniques for robust GNSS carrier tracking," in *Proceedings of the ION GNSS 2017*, Portland, OR, USA, 2017, pp. 25–29, Institute of Navigation.

[30] J. H. Won, "A novel adaptive digital phase lock loop for modern digital GNSS receivers," *IEEE Communications Letters*, vol. 17, no. 2, pp. 393–396, 2013.

[31] C. O. Driscoll and G. Lachapelle, "Comparison of traditional and Kalman filter based tracking architectures," in *Proc. of European Navigation Conference 2009 (ENC09)*, Naples, Italy, 2009, pp. 100–110, European Navigation Conference 200.

[32] J. H. Won, T. Pany, and B. Eissfeller, "Characteristics of Kalman filter approach for signal tracking loop of GNSS receiver," *IEEE Aerospace and Electronics Systems*, vol. 48, no. 4, pp. 3671–3681, 2012.

[33] P. W. Ward, "Using a GPS receiver monte carlo simulator to predict RF interference performance," in *Proceedings of ION GPS*, Kansas City, MO, September 1997, pp. 1473–1482.

[34] J. W. Betz, "Effect of narrowband interference on GPS code tracking accuracy," in *Proccedings of the ION NTM*, Anaheim, CA, 2003, pp. 16–27, Institute of Navigation.

[35] T. N. Morrissey, K. W. Shallberg, A.J. Van Dierendonck, and M.J. Nicholson, "GPS receiver performance characterization under realistic ionospheric phase scintillation environments," *Radio Science*, vol. 39, no. 2, pp. 1–18, 2004.

[36] Todd E. Humphreys, Mark L. Psiaki, Paul M. Kintner Jr., and Brent M. Ledvina, "GPS carrier tracking loop performance in the presence of ionospheric scintillations," in *Proceedings of the ION GNSS 2005*, Long Beach, CA, 2005, pp. 156 – 167, Institute of Navigation.

[37] P. H. Doherty, S. H. Delay, C. E. Valladares, and J. A. Klobuchar, "Ionospheric scintillation effects in the equatorial and auroral regions," in *Proceedings of the ION GNSS 2000*, Salt Lake City, Utah, USA, 2000, Institute of Navigation.

[38] C. S. Carrano, K. M. Groves, W. J. McNeil, and P. H. Doherty, "Scintillation characteristics across the GPS frequency band," in *Proc. of ION ITM*, Nashville, TN, 2012, pp. 1972–1989, ION.

[39] S. H. Delay, C. S. Carrano, K. M. Groves, and P. H. Doherty, "A statistical analysis of GPS L1, L2, and L5 tracking performance during ionospheric scintillation," in *Proc. of ION Pacific PNT Conference 2015*, Honolulu, HI, 2015, p. 1, ION.

[40] K. Borre, D. M. Akos, N. Bertelsen, P. Rinder, and S.H. Jensen, *A software-defined GPS and Galileo receiver: a single-frequency approach*, Birkhauser, Boston, 2007.